Journal of Theoretical and Applied Physics (2020) 14:367–376
https://doi.org/10.1007/s40094-020-00393-2

RESEARCH

Tunable and reversible thermo-plasmonic hot spot imaging for temperature confinement

N. S. Shnan[1,2] · N. Roostaei[1] · S. M. Hamidi[1]

Received: 26 July 2020 / Accepted: 4 September 2020 / Published online: 18 September 2020

Abstract

In the present study, a novel tunable two-dimensional thermo-plasmonic grating based on gold nanorods was demonstrated by combining the plasmonic properties of the gold nanostructure and the applied external voltage. In this structure, a thin layer of the gold grating was typically deposited on a patterned polydimethylsiloxane substrate using the nanoimprint lithography method. The surface plasmon resonance of the fabricated plasmonic structure was excited by the surface plasmon imaging system based on a high numerical aperture objective lens and the charged coupled device camera. Based on the results, the number of the plasmonic hot spots due to the thermo-plasmonic effect increased by the external voltage, leading to an increase in this effect. Therefore, this reversible and tunable temperature confinement can be used as the controller of each element including cells in a defined micro-position.

Keywords Plasmonic imaging system · Plasmonic hot spot · 2D grating · Nanoimprint lithography · Temperature confinement

Introduction

Plasmonic nanostructures have been proposed as a new efficient heat source when illuminated by their correspondence resonance light source [1, 2] regarding the nanoscale control of temperature distribution [3], drug delivery [4, 5], cancer photo-thermal therapy [6, 7], photo-thermal imaging [8], and various other useful applications. These applications should be capable of measuring the temperature distribution in a sufficient area with a high signal-to-noise ratio (SNR).

Nowadays, different evidence is available concerning the metal nanoparticle-based structure for satisfying the abovementioned SNR in the temperature distribution, resulting in introducing novel development in chemistry and biology while not in the physics [9]. All these evaluations aim to establish a better understanding about the physical phenomenon such as the thermo-plasmonic effect in nanoparticle-based structures [10], nanorod-based structures [11], and self-assembled nanoparticles [12] in order to have preferable SNR onto the arrays of nanoparticles [13]. The proposed arrays can solve the SNR in the large area of the nanostructure for helping interested scientists. In addition, reports exist onto an optical microscopy technique in order to quantitatively map the temperature distribution around the nanometric sources of heat by experimental and simulation results [14]. Although it is considered as the best use of plasmon-based localization in these new kinds of nano-sources of heat, controlling this heating amount, and supported area remains unknown. In other words, the ability to control and tune the thermo-plasmonic effect is extensively useful for all of the abovementioned applications.

On the other hand, the most applicable methods for tuning plasmon-driven reactions include the use of liquid crystals [15–17], piezoelectric materials [18], magneto-plasmonic structures [19], or the use of external voltage for obtaining voltage-induced surface plasmon resonance [20, 21]. Although the thermo-plasmonic effect is one of the plasmon-driven reactions, no evidence is available regarding the abovementioned effects, mainly external voltage onto this highly useful phenomenon.

Accordingly, to the best of our knowledge, the present study first evaluated the effect of this external parameter

✉ S. M. Hamidi
m_hamidi@sbu.ac.ir

[1] Magneto-plasmonic Lab, Laser and Plasma Research Institute, Shahid Beheshti University, Tehran, Iran

[2] Department of Laser Physics, College of Science for Woman, University of Babylon, Babylon, Iraq

onto the thermo-plasmonic and plasmonic hot spots using the common plasmon imaging system.

Experimental part

Sample preparation

The main sample including polydimethylsiloxane material (PDMS) as a substrate and 35 nm of gold as a plasmonic substance was prepared by soft lithography processes (Fig. 1). To this aim, 0.2 g of PDMS, along with 0.02 g of curing agent at a weight ratio of 1:10, was used onto the two-dimensional (2D) charged coupled camera (CCD) as the main stamp. After placing the CCD in a frame and adding the PDMS mixture onto the CCD, the sample was placed in a vacuum chamber for 15 min in order to avoid the formation of air bubbles and coating the gold cover layer as extensively explained in our previous study [22].

Figure 2a illustrates the *scanning electron microscope* image of the 2D plasmonic grating in a simple cubic structure and the unit cell sizes of about 1.2 µm, as well as the nanowires between each cube and the displacement of the crystal period.

Plasmonic imaging system

The schematic layout of the optical imaging system and the real image of the sample is shown in Fig. 2b, c. Based on these data, the green laser beam with a wavelength of 532 nm was divided into two equal parts by a beam splitter. Then, the sample was illuminated by an objective lens with a numerical aperture set to 1.25, and the reflected light of the sample was received by. Finally, the image of the sample was collected by the lens of the focal length of 6.5 cm before the CCD camera.

Considering that the present plasmonic nanostructure is formed by a 2D array of gold nanowires, it can support narrow diffracted orders and localized plasmon resonances in far-field measurements leading to surface lattice resonance as explained in our previous studies [15, 23].

The objective lens with a high numerical aperture can be used to excite surface plasmon polariton (SPP). Further, the high numerical aperture of the objective ensures that the sample is illuminated in a wide range of supercritical angles and the total internal reflection phenomenon occurs which is explained in the next section.

Excitation of surface plasmon polaritons (SPPs) by an objective lens

An objective lens with a high numerical aperture (NA > 1) can be used for SPP excitation. In SPP microscopes, the spatial resolution of imaging is limited by the SPP propagation length. Thus, the spatial resolution improves if the excitation of SPPs is localized over a smaller area.

As shown in Fig. 3, an oil-immersion objective through the oil layer is connected with the surface of the sample and

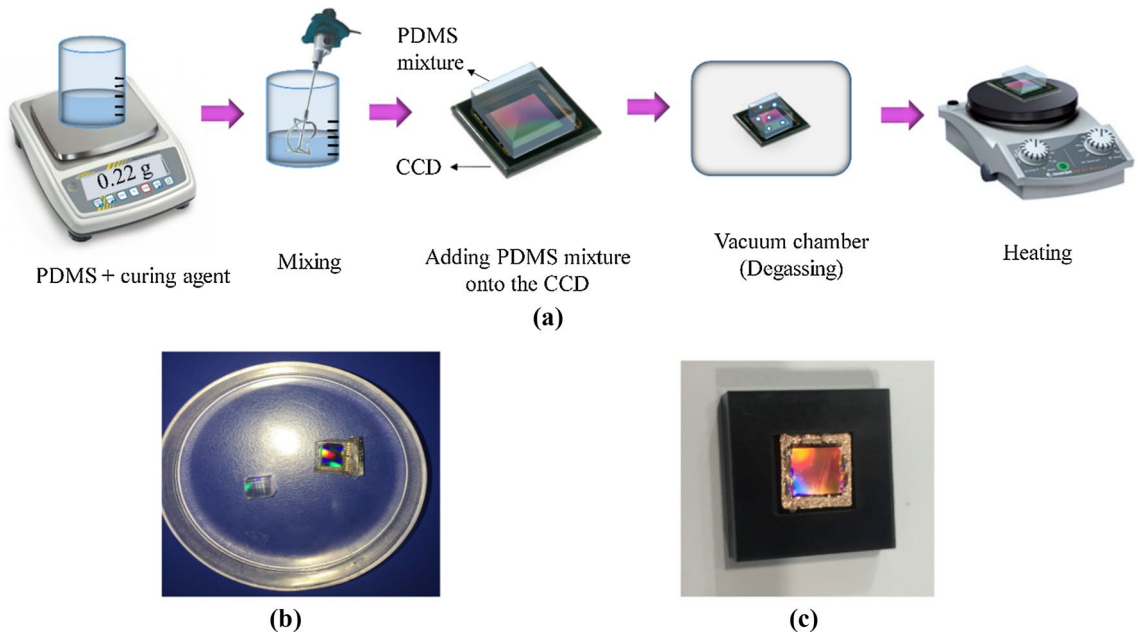

Fig. 1 Sample preparation steps **a** a schematic of the fabrication process of PDMS substrate, **b** polymer structure separated from CCD and **c** the prepared sample after the deposition of gold onto the PDMS substrate

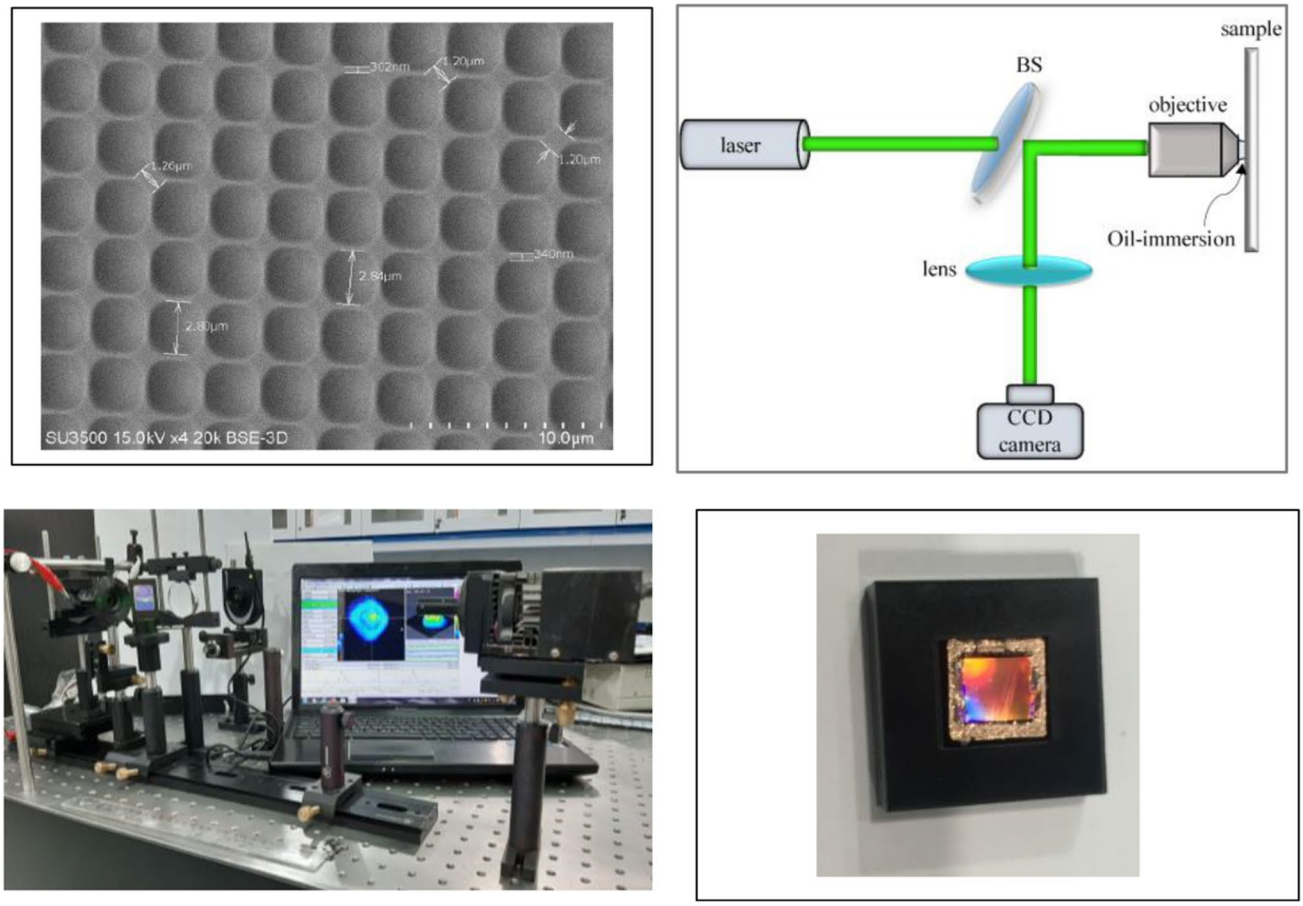

Fig. 2 **a** SEM image of the sample, **b** schematic array of the plasmonic imaging systems, **c** the real image of the experimental setup and **d** the real image of the prepared sample

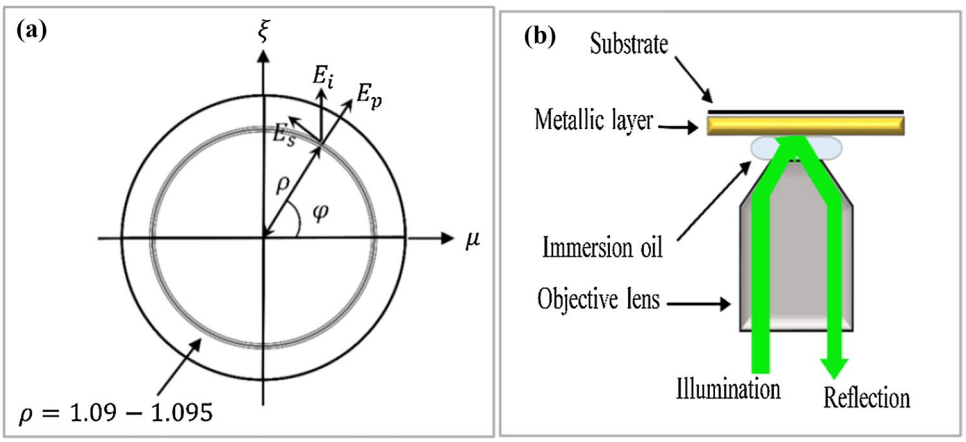

Fig. 3 **a** Schematic of the SPPs excitation using an objective lens with a high numerical aperture and **b** the coordinate of the pupil plane of the objective lens

the light is focused by the objective lens at the interface between the substrate and the metallic film.

Furthermore, the high numerical aperture of the objective satisfies the dispersion matching condition between the light and SPP. The propagation constant of excited SPPs on the metal surface is expressed by Eq. (1) as follows:

$$k_{sp}(\omega) = \frac{\omega}{c}\sqrt{\frac{\varepsilon_1(\omega)\varepsilon_2(\omega)}{\varepsilon_1(\omega)+\varepsilon_2(\omega)}} \tag{1}$$

where ω and c represent the angular frequency and the light speed in the vacuum, respectively. Additionally, $\varepsilon_1(\omega)$ and $\varepsilon_2(\omega)$ are the relative permittivities of the metal and air, respectively. The propagation constant of light propagating in the air is given as follows:

$$k_{light}(\omega) = \frac{\omega}{c}\sqrt{\varepsilon_2(\omega)} \tag{2}$$

In typical cases, the ratio of k_{sp} to k_{light} is approximately 1.05–1.10. Therefore, the required light for SPP excitation should be an evanescent wave which has a propagation constant of 1.05–1.10 times greater than that of light propagating in the air. This necessary evanescent wave can be produced using an objective lens with a high numerical aperture. The present study used the linearly polarized light with a wavelength of 532 nm and assumed a gold film with a thickness of 35 nm as a metallic film and an objective lens with NA = 1.25. In addition, the relative permittivity of gold at $\lambda = 532$ nm was $\varepsilon_1 = -4.6810 + 2.4266i$. By calculating the ratio of $k_{sp}(\omega)$ to $k_{light}(\omega)$, the ring size or NA range can be obtained in which the dispersion matching condition was satisfactory (in our case, NA range = 1.09–1.095).

In addition, the electric field distribution on the metal surface should be calculated for accurate evaluations. First, the incident electric field at the entrance pupil of the objective lens was calculated in this study. The incident light exists in the shaded area ($1.09 < \rho < 1.095$) which corresponds to NA = 1.09–1.095.

When the linearly polarized light incidences are on the pupil plane of the objective lens, electric field components (i.e., *p*- and *s*-polarized) at the pupil plane are represented by Eq. (3) as follows:

$$\begin{aligned} &E_p(\rho,\varphi) = E_i\cos\varphi(1.09 < \rho < 1.095)\\ &E_s(\rho,\varphi) = E_i\sin\varphi(1.09 < \rho < 1.095)\\ &E_p(\rho,\varphi),\quad E_s(\rho,\varphi) = 0 \qquad\qquad (\text{otherwise}) \end{aligned} \tag{3}$$

where E_i denotes the amplitude of the incident electric field and ρ and φ demonstrate radial and azimuthal coordinates at the pupil plane, respectively. The light passing from any particular position (ρ, φ) of the pupil plane is converted to a corresponding plane wave by the objective lens and illuminates the sample. The amplitude transmission coefficient of the system of such three layers is written as Eq. (4) as follows:

$$T_m(\rho) = \frac{t_{01}^m(\rho)t_{12}^m(\rho)\exp\left[ik_{1z}(\rho)d_1\right]}{1 - r_{10}^m(\rho)r_{12}^m(\rho)\exp\left[i2k_{1z}(\rho)d_1\right]} m = p, s. \tag{4}$$

where r_{ab}^m and t_{ab}^m are the Fresnel reflection and transmission coefficient at an interface of mediums a and b for the light which is incident from medium a. Further, k_{1z} and d_1 denote the z component of a wave vector in the Au layer and the thickness of the Au layer, respectively.

The amplitude components produced by light passing the position (ρ, φ) of the pupil plane are obtained from Eqs. (3) and (4). Thus, functions E_ρ^{SPP}, E_φ^{SPP} and E_z^{SPP} are introduced to represent the components which oscillate in the radial (ρ), azimuthal (φ), and z directions in the sample [24]. Finally, the intensity I^{SPP} of the electric field in the sample is obtained by integrating the amplitude which is produced by each plane wave with respect to the oscillation direction.

$$\begin{aligned} I^{SPP}(x,y) = &\left|\int E_x^{SPP}(x,y,\rho,\varphi)\rho\mathrm{d}\rho\mathrm{d}\varphi\right|^2\\ &+\left|\int E_y^{SPP}(x,y,\rho,\varphi)\rho\mathrm{d}\rho\mathrm{d}\varphi\right|^2\\ &+\left|\int E_z^{SPP}(x,y,\rho,\varphi)\rho\mathrm{d}\rho\mathrm{d}\varphi\right|^2. \end{aligned} \tag{5}$$

The imaging process for the 2D structure of PDMS/Au nanorods was used after the alignment of light in the optical system. It is worth noting that this arrangement can switch from real to Fourier space and vice versa by changing the distance between the objective lens and the sample. These measurements were conducted without any external voltage and under external voltage with different passed currents which were affected by varied frequencies.

Results and discussion

The recorded Fourier and real images of the 2D structure of PDMS-Au are shown in Figs. 4A and B, respectively. The zoomed picture of the main part of the Fourier image is observed in the inset of Fig. 4a, which confirms the C4 symmetry group of the present 2D sample. Furthermore, the image of plasmonic hot spots for the real part is illustrated in Fig. 4C. Based on the data, the SPPs are excited by the

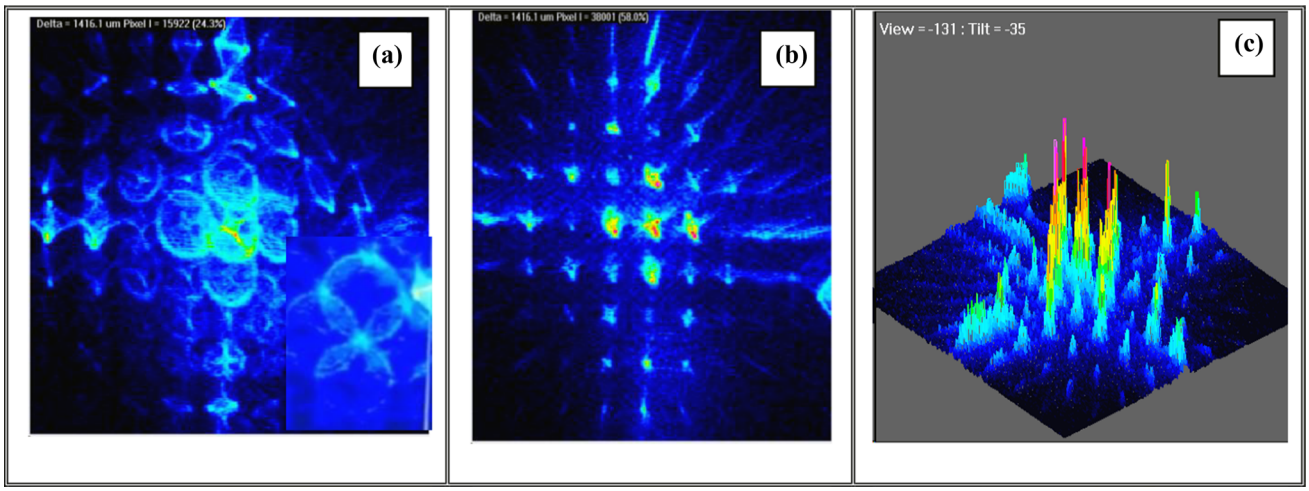

Fig. 4 The CCD images of the two-dimensional sample PDMS-Au, **a** Fourier image, **b** real image and **c** hotspot image; the inset in the **a** shows the zoomed main part of Fourier image

Table 1 Values of applied frequencies and voltages on the sample 1

Frequency (MHz)	Voltage (V)	Voltage (V)	Voltage (V)
$f_1 = 1.2$	$V_{min} = 2169*10^{-6}$	$V_{mid} = 4680*10^{-6}$	$V_{max} = 239.4*10^{-3}$
$f_2 = 2.2$	$V_{min} = 14{,}040*10^{-6}$	$V_{mid} = 29{,}970*10^{-6}$	$V_{max} = 34{,}434*10^{-6}$
$f_3 = 3.2$	$V_{min} = 12{,}330*10^{-6}$	$V_{mid} = 22{,}140*10^{-6}$	$V_{max} = 30{,}150*10^{-6}$

objective lens and can initiate radiation. Thus, they can be observed through their radiation.

After recording the Fourier and real image of the sample, plasmonic hot spots under external voltage received attention, followed by investigating the voltage-induced plasmonic hot spot in these samples. For this purpose, different values of voltage and frequency were applied on Samples 1 and 2, and the images of plasmonic hot spots were recorded using the imaging system. Furthermore, three different frequencies were selected and three different values of voltages as the minimum, middle, and maximum were applied for each frequency (Table 1).

Based on the results in Fig. 5, the excitation of SPP represents an increase by increasing the apply voltage, leading to an increase in intensity, which occurs since the SPP relies on the dielectric constants of metal (Au) and dielectric (PDMS), and these constants (ε_1, ε_2) change by applying the voltage. The experimental results demonstrated the effect of the applied frequency on SPP excitation considering that the frequency of the applied voltage is affected on SPP frequency. Based on experimental findings, the best result and high excitation were observed when the frequency $f = 2.2$ MHz for Sample 1. Accordingly, the number of plasmonic hot spots increases and the thermo-plasmonic phenomenon occurs by applying voltage.

The histogram of the change in the intensity in x and y directions was extracted to obtain a better understanding of the physical change in the sample under external voltage (Fig. 6a–c). Based on the presented data, the intensity and plasmonic hot spot increase by applying voltage. Additionally, it is physically approved that the thermo-plasmonic phenomenon occurs by employing voltage.

In addition, the sample experienced extremely sharp enhancement in the number and intensity of the hot spot in both x and y directions. The increase occurred for applied voltage from 12 to 30 mV at 3.2 MHz due to the increased current from 1.3 to 3.3 mA (Fig. 6a). This trend is repeated for the middle frequency (2.2 MHz) from 1.5 to 3.8 mA (Fig. 6b). An increase in the number of the hot spot and the area under the curve for the maximum value of the applied voltage in this frequency is highly surprising, which is repeated and amplified for the last frequency set to 1.2 MHz by the applied current from 2.41 µA to 26.6 mA (Fig. 6c).

It is well known that thermo-plasmonic phenomena exist which linearly improves by increasing the current due to a decrease in the applied frequency due to the current flow

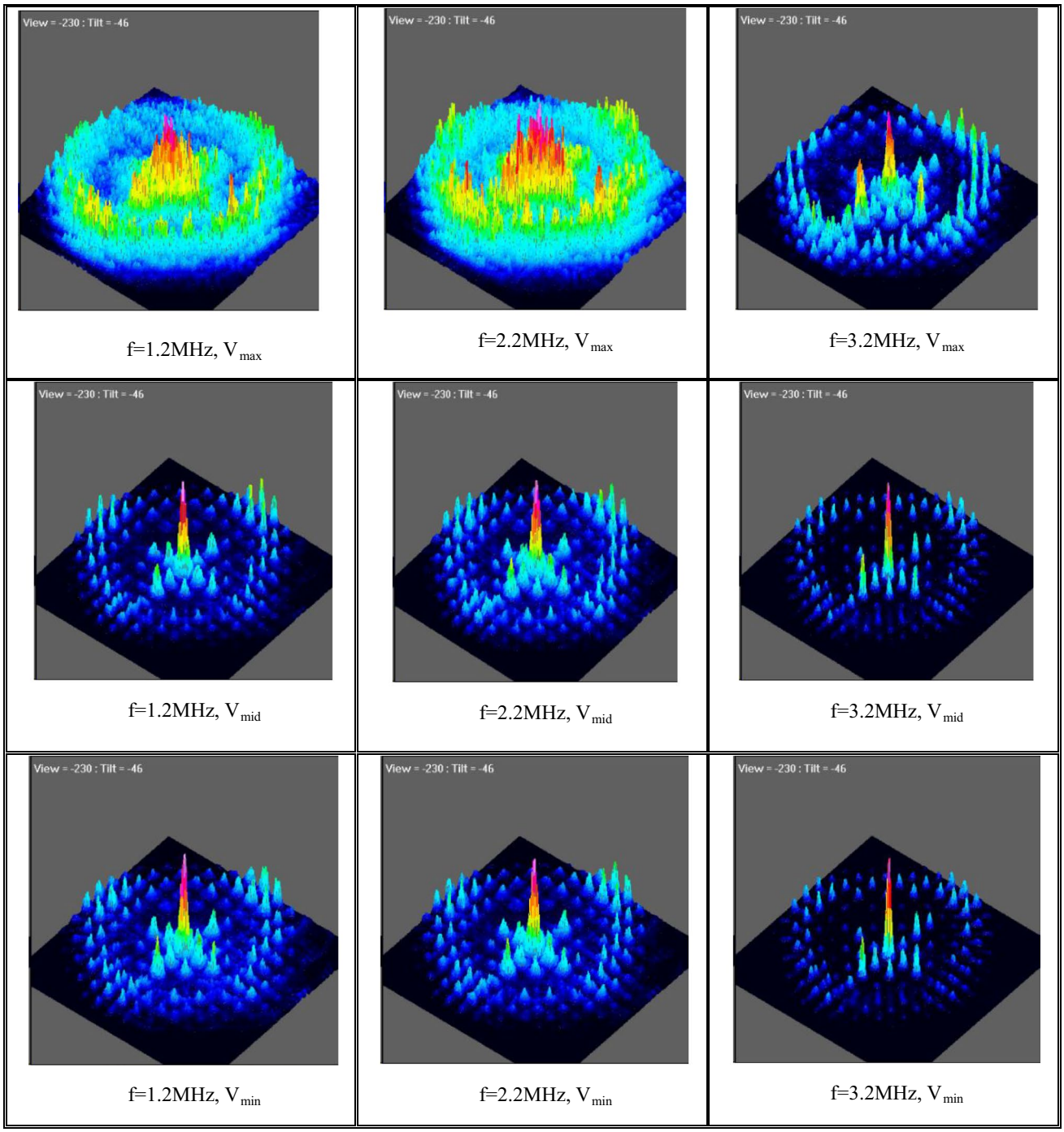

Fig. 5 Hotspot for sample 1 for different value of frequency and voltage

in the gold thin grating. In other words, voltage-induced thermo-plasmonic occurs in this sample and it is measured which is highly useful in thermo medical applications. The heat generation at each motif of the 2D plasmonic structure

Fig. 6 Hotspot intensity distribution for sample 1 in *X* (left graph) ▶ and *Y* (right graph) dimensions and 2D graph from minimum (bottom) to maximum (top) value of applied voltage (center graph) for **a** f = 3.2 MHz, **b** *f* = 2.2 MHz and **c** f = 1.2 MHz

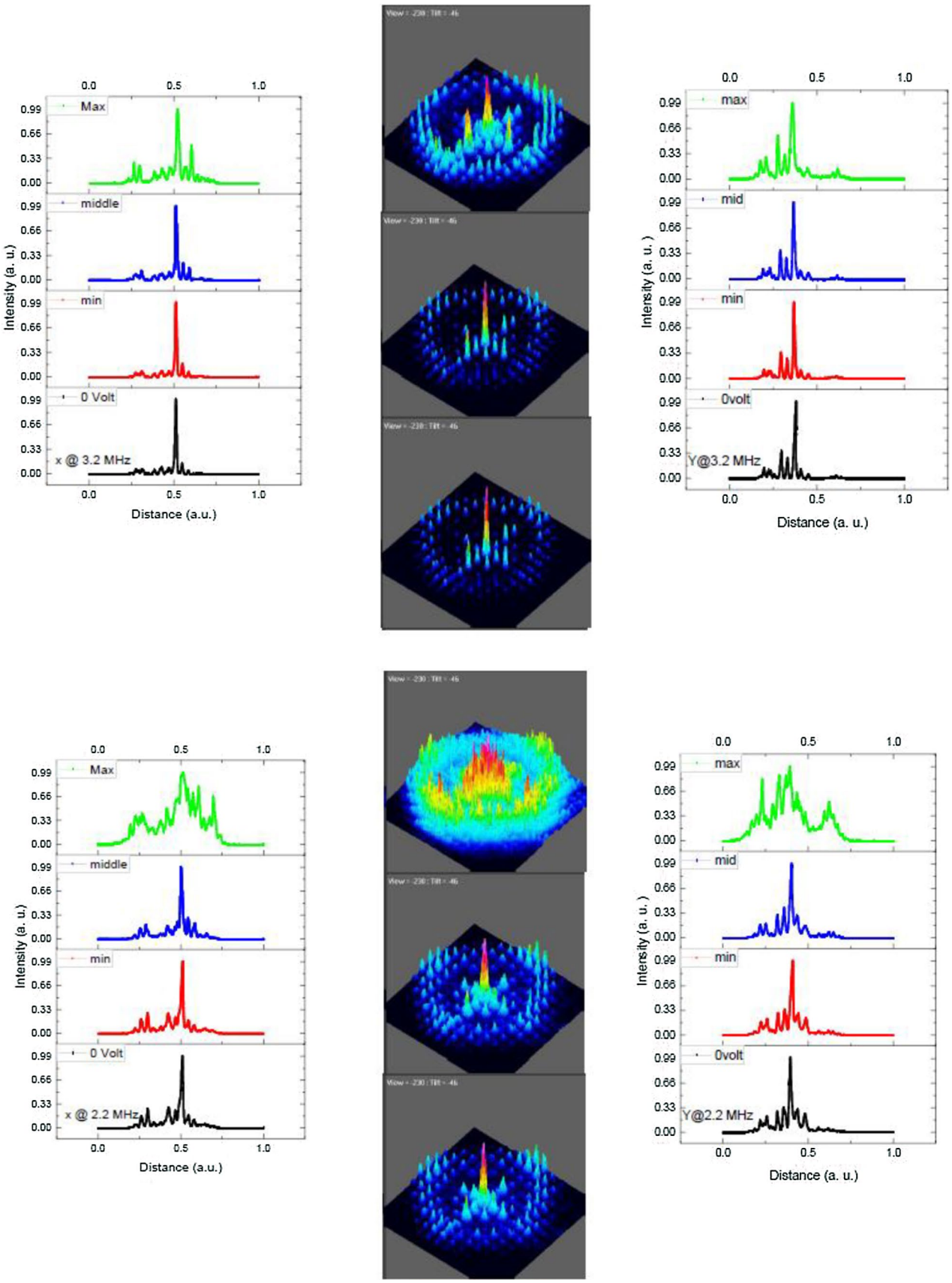
Max
middle
min
0 Volt
x @ 3.2 MHz
Intensity (a. u.)
Distance (a.u.)
max
mid
min
0volt
Y@3.2 MHz
Distance (a. u.)
Max
middle
min
0 Volt
x @ 2.2 MHz
Intensity (a. u.)
Distance (a.u.)
max
mid
min
0volt
Y@2.2 MHz
Distance (a. u.)

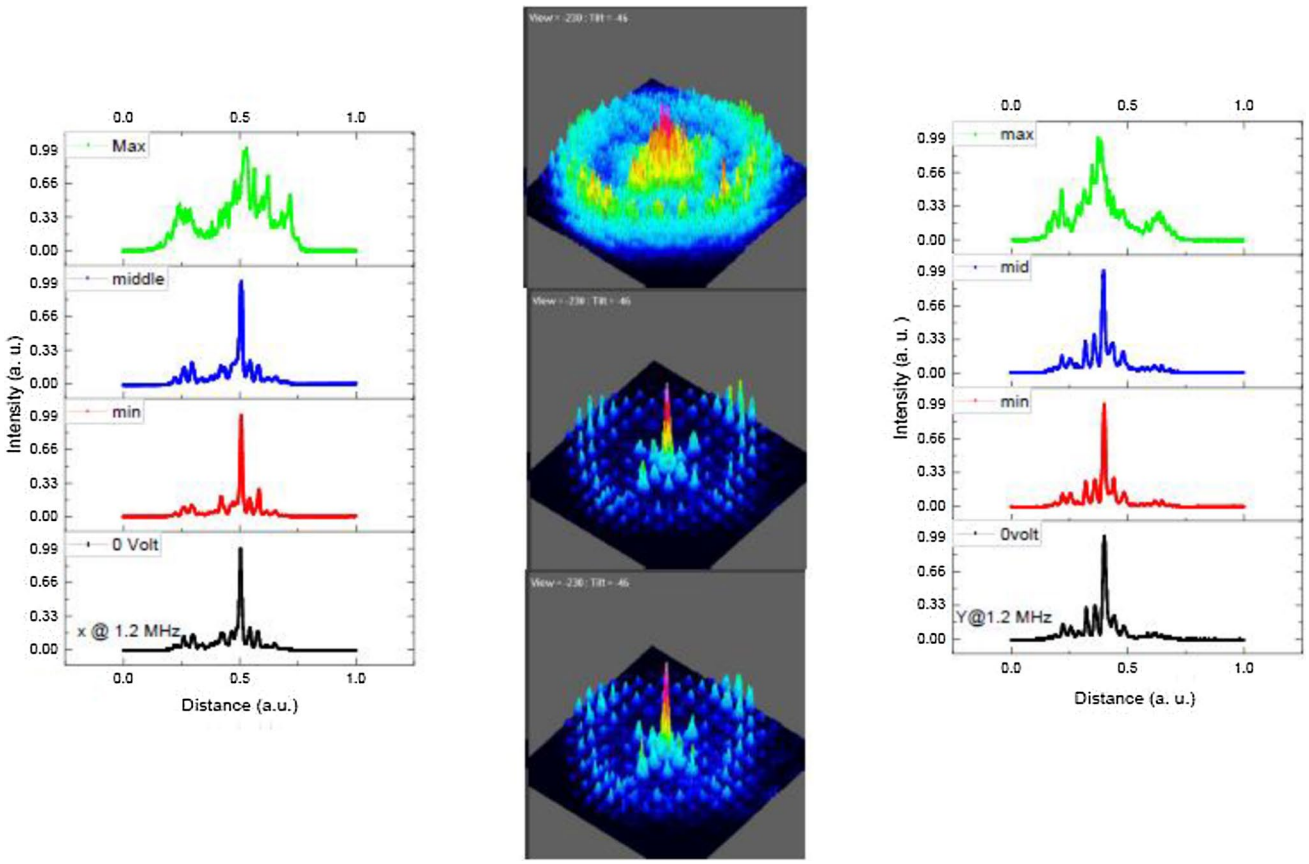

Fig. 6 (continued)

Table 2 Values of applied frequencies and voltages on the sample 2

Frequency (kHz)	Voltage (V)	Voltage (V)	Voltage (V)
$f=100$	$V_{min}=433*10^{-3}$	$V_{mid}=3.3$	$V_{max}=7.4$

is directly observed by counting the number of hot spots in each x or y direction. In other words, the temperature distribution in the gold nanorods is found to be localized hot spots in the middle part of each graph for different applied voltages. Further, the intensity in the histogram of x and y directions can be connected to the temperature distributions throughout the periodic lattices of nanorods.

These results highlight the high degree of temperature confinement at each motif site and the ability to tune the degree of temperature confinement by frequency and voltage in each category. Accordingly, this enhancement factor can be can extended over 33% (0.33 in the intensity) for the maximum voltage in two later cases in order to use them for photo-thermal therapy applications.

As shown, there is a trade-off between these two properties. For example, the degree of temperature confinement reduces while obtaining a higher temperature by increasing the voltage. To this end, another sample with a slight increase in the gold grating thickness to 45 nm was evaluated, and thus the resistance of the sample increased to obtain lower current flow. Considering this change in the resistance, the sample flows from 14 to 216 μA from the minimum to maximum applied voltage at 100 kHz (Table 2).

The hot spot histogram in both x and y directions of the sample and the 2D graph of this plasmonic excitation are depicted in Fig. 7. As illustrated, no sufficient change is observed in the thermo-plasmonic hot spot distribution due to the same order in the flowed current from the sample. As explained earlier, a high degree of temperature confinement was observed when comparing this sample with the first one. This reversible temperature confinement can be used as the controller of each element including the cells in a defined micro-position.

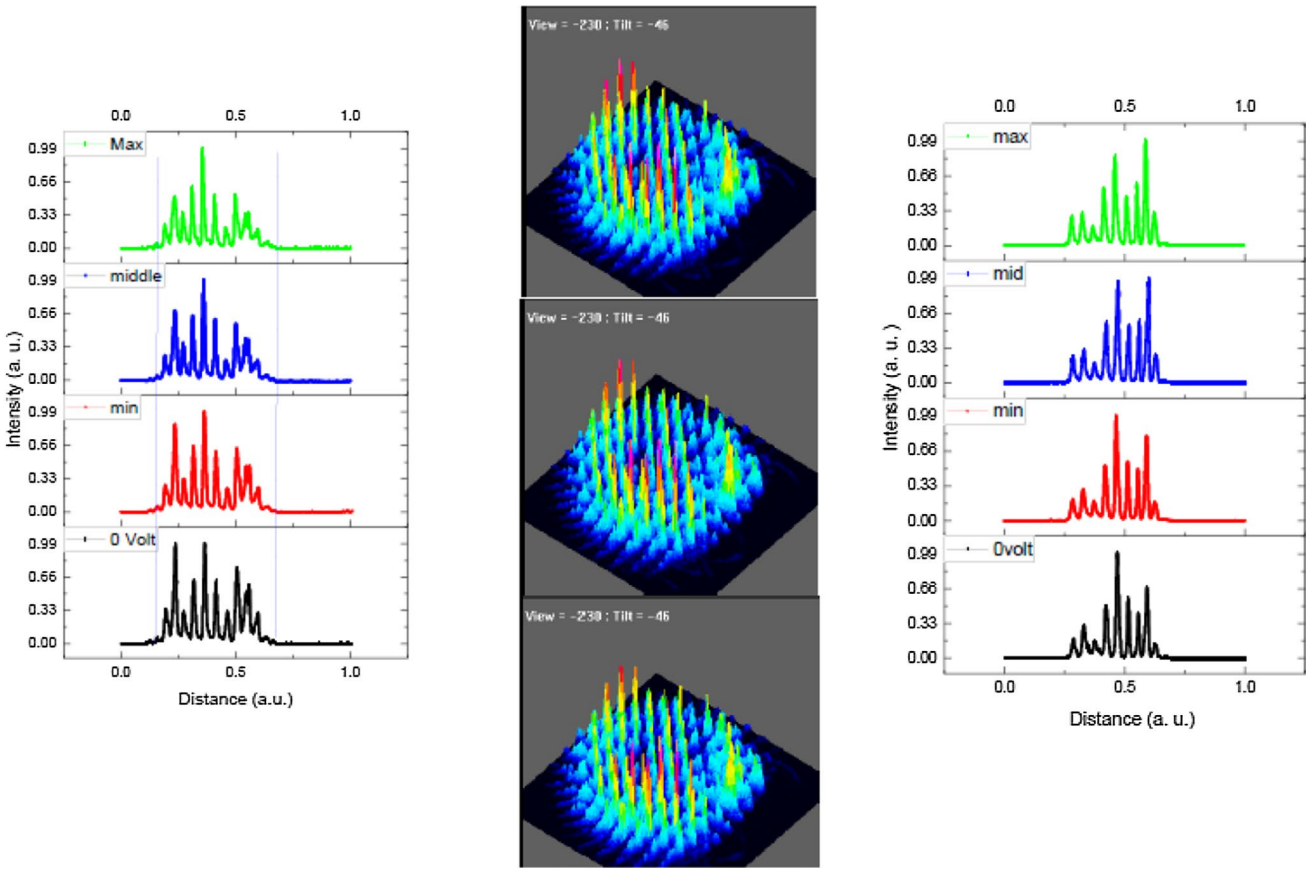

Fig. 7 Hotspot intensity distribution for sample 1 in *X* (left graph) and *Y* (right graph) dimensions and 2D graph from minimum (bottom) to maximum (top) value of applied voltage (center graph) for $f = 100$ kHz

Conclusion

In general, the present study reported cost-effective thermo-plasmonic samples based on the arrays of gold nanorods by the nanoimprint lithography process. In this approach, the surface plasmon excitation setup was used based on the objective lens in order to obtain plasmonic hot spot distribution in both Fourier and real images under the externally applied voltage. Based on the findings, the Fourier image appeared as bright disks relying on the optical axis and the distance from outward to the center of the disk proportional to NA. The applied voltage caused the rapid heating of nanorods, leading to a quick increase in the temperature due to the thermo-plasmonic effect. In addition, the degree of temperature confinement could be controlled by a change in the resistivity of the sample, and the passed current from the sample. More precisely, tunable thermo-plasmonic was obtained by the applied voltage in each frequency category and adjustable temperature confinement by changing the pass current of the sample which is extremely useful in photo-thermal applications.

Compliance with ethical standards

Conflict of interest There is no any conflicts of interest between authors.

References

1. Rodríguez-Oliveros, R., Sánchez-Gil, J.A.: Gold nanostars as thermoplasmonic nanoparticles for optical heating. Opt. Express **20**(1), 621–626 (2012)
2. Baffou, G., Quidant, R.: Thermo-plasmonics: using metallic nanostructures as nano-sources of heat. Laser Photonics Rev. **7**(2), 171–187 (2013)
3. Baffou, G., Quidant, R., Javier García de Abajo, F.: Nanoscale control of optical heating in complex plasmonic systems. ACS Nano **4**(2), 709–716 (2010)
4. Han, G., Ghosh, P., De, M., Rotello, V.M.: Drug and gene delivery using gold nanoparticles. NanoBiotechnology **3**(1), 40–45 (2007)
5. Han, G., Ghosh, P., De, M., Rotello, V.M.: Gold nanoparticles in delivery applications. Adv. Drug Deliv. Rev. **60**(11), 1307–1315 (2008)
6. Choi, J., Yang, J., Jang, E., Suh, J.-S., Huh, Y.-M., Lee, K., Haam, S.: Gold nanostructures as photothermal therapy agent for cancer. Anticancer Agents Med. Chem. **11**(10), 953–964 (2011)
7. Ahmad, R., Fu, J., He, N., Li, S.: Advanced gold nanomaterials for photothermal therapy of cancer. J. Nanosci. Nanotechnol. **16**(1), 67–80 (2016)
8. Boyer, D., Tamarat, P., Maali, A., Lounis, B., Orrit, M.: Photothermal imaging of nanometer-sized metal particles among scatterers. Science **297**(5584), 1160–1163 (2002)
9. Cao, L., Barsic, D.N., Guichard, A.R., Brongersma, M.L.: Plasmon-assisted local temperature control to pattern individual semiconductor nanowires and carbon nanotubes. Nano Lett. **7**(11), 3523–3527 (2007)
10. Palermo, G., Cataldi, U., Pezzi, L., Bürgi, T., Umeton, C., De Luca, A.: Thermo-plasmonic effects on E7 nematic liquid crystal. Mol. Cryst. Liq. Cryst. **649**(1), 45–49 (2017)
11. Herzog, J.B., Knight, M.W., Natelson, D.: Thermoplasmonics: quantifying plasmonic heating in single nanowires. Nano Lett. **14**(2), 499–503 (2014)
12. Gatea, M.A., Jawad, H.A., Hamidi, S.M.: Detecting the thermoplasmonic effect using ellipsometry parameters for self-assembled gold nanoparticles within a polydimethylsiloxane matrix. Appl. Phys. A **125**(2), 103 (2019)
13. Baffou, G., Berto, P., BermúdezUreña, E., Quidant, R., Monneret, S., Polleux, J., Rigneault, H.: Photoinduced heating of nanoparticle arrays. ACS Nano **7**(8), 6478–6488 (2013)
14. Baffou, G., Bon, P., Savatier, J., Polleux, J., Zhu, M., Merlin, M., Rigneault, H., Monneret, S.: Thermal imaging of nanostructures by quantitative optical phase analysis. ACS Nano **6**(3), 2452–2458 (2012)
15. Mbarak, H., Hamidi, S.M., Mohajerani, E., Zaatar, Y.: Electrically driven flexible 2D plasmonic structure based on a nematic liquid crystal. J. Phys. D Appl. Phys. **52**(41), 415106–415110 (2019)
16. Palermo, G., Cataldi, U., De Sio, L., Bürgi, T., Tabiryan, N., Umeton, C.: Optical control of plasmonic heating effects using reversible photo-alignment of nematic liquid crystals. Appl. Phys. Lett. **109**(19), 191906 (2016)
17. Palermo, G., Sio, L.D., Placido, T., Comparelli, R., Curri, M.L., Bartolino, R., Umeton, C.: Plasmonic thermometer based on thermotropic liquid crystals. Mol. Cryst. Liq. Cryst. **614**(1), 93–99 (2015)
18. Kodeary, A., Hamidi, S.M.: Tunable piezophotonic effect on core–shell nanoparticles prepared by laser ablation in liquids under external voltage. J. Nanotechnol. (2019). https://doi.org/10.1155/2019/6046079
19. Hamidi, S.M., Mosaeii, B., Afsharnia, M., Aftabi, A., Najafi, M.: Magneto-plasmonic study of aligned Ni, Co and Ni/Co multilayer in polydimethylsiloxane as magnetic field sensor. J. Magn. Magn. Mater. **417**, 413–419 (2016)
20. Chu, K.C., Chao, C.Y., Chen, Y.F., Wu, Y.C., Chen, C.-C.: Electrically controlled surface plasmon resonance frequency of gold nanorods. Appl. Phys. Lett. **89**(10), 103107 (2006)
21. Hoang, T.B., Mikkelsen, M.H.: Broad electrical tuning of plasmonic nanoantennas at visible frequencies. Appl. Phys. Lett. **108**(18), 183107 (2016)
22. Asgari, N., Hamidi, S.M.: Exciton-plasmon coupling in two-dimensional plexitonic nano grating. Opt. Mater. **81**, 45–54 (2018)
23. Haddawi, S.F., Mirahmadi, M., Mbarak, H., Kodeary, A.K., Ghasemi, M., Hamidi, S.M.: Footprint of plexitonic states in low power green blue plasmonic random laser. Appl. Phys. A **125**(12), 843–846 (2019)
24. Kano, H., Mizuguchi, S., Kawata, S.: Excitation of surface-plasmon polaritons by a focused laser beam. JOSA B **15**(4), 1381–1386 (1998)